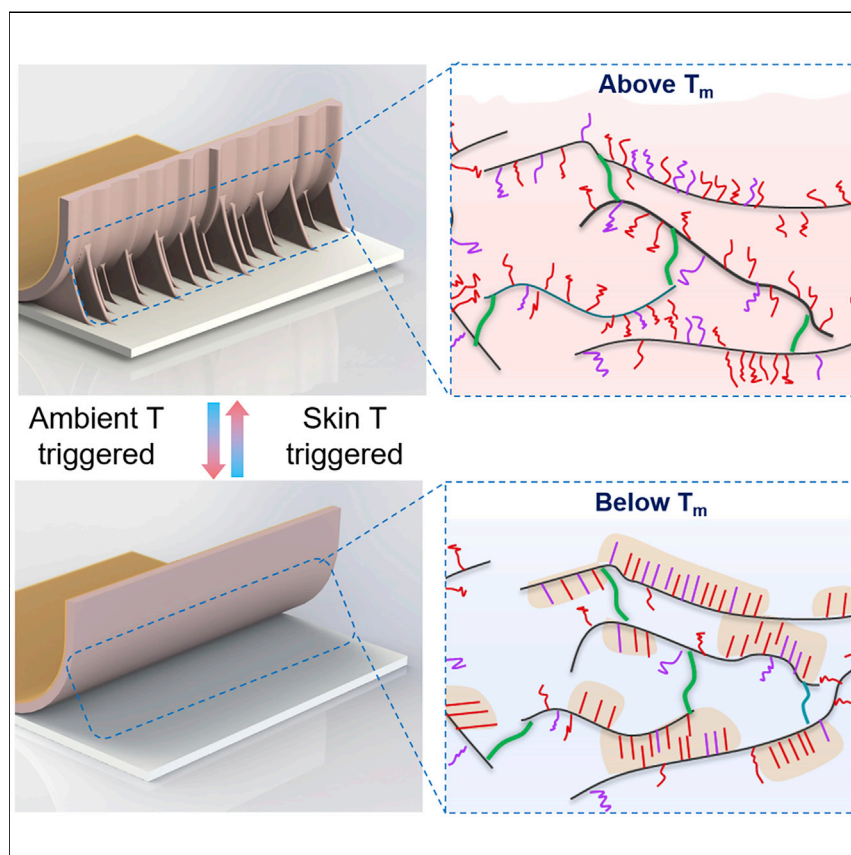


Article

Skin temperature-triggered, debonding-on-demand sticker for a self-powered mechanosensitive communication system



Bistable adhesive polymer (BAP) with skin temperature-triggered conformal adhesion and room temperature-triggered easy detaching is explored as a debonding-on-demand biocompatible skin adhesive. Based on the BAP substrate, an optically transparent and mechanically compliant debonding-on-demand triboelectric nanogenerator is fabricated, which could serve as a human-machine interface for self-powered drone navigation. This demonstrates the potential applications of the BAP for smart artificial skins, soft robots, and self-powered biomechanical monitoring systems.

Meng Gao, Hanxiang Wu, Roshan Plamthottam, ..., Lily Wu, Ximin He, Qibing Pei

qpei@seas.ucla.edu

Highlights

A biocompatible reusable debonding-on-demand skin adhesive

Conformal and compliant adhesion on skin

Easy detaching at room temperature or with tap water

A reversible adhesive-based human-machine interface for self-powered drone navigation

**Demonstrate**

Proof-of-concept of performance with intended application/response

Gao et al., Matter 4, 1–13
June 2, 2021 © 2021 Elsevier Inc.
<https://doi.org/10.1016/j.matt.2021.03.003>

Article

Skin temperature-triggered, debonding-on-demand sticker for a self-powered mechanosensitive communication system

Meng Gao,^{1,3,4} Hanxiang Wu,^{1,4} Roshan Plamthottam,¹ Zhixin Xie,¹ Ying Liu,¹ Junhui Hu,² Shuwang Wu,¹ Lily Wu,² Ximin He,¹ and Qibing Pei^{1,5,*}

SUMMARY

In the field of skin-attachable electronics, debonding-on-demand (DoD) adhesives triggered by mild, efficient, and accessible stimuli can facilitate repeated usage with negligible damage to the skin. Here, a simple and versatile method has been developed to fabricate biocompatible bonding/debonding bistable adhesive polymers (BAPs) with skin temperature-triggered conformal adhesion and room temperature-triggered easy detaching. Its potential application in a mechanosensitive communication system is also explored. The BAPs are designed by incorporating stearyl acrylate (SA) and tetradecyl acrylate (TA) into a chemically crosslinked elastomer, where a semicrystalline-to-amorphous transition between 26°C and 32°C results in high adhesive flowability and large energy dissipation. An optically transparent and mechanically compliant debonding-on-demand triboelectric nanogenerator (DoD-TENG) is fabricated using the BAP as the DoD substrate, a polydimethylsiloxane elastomer as the electrification layer, and an ion-conductive elastomer as the electrode. Furthermore, the DoD-TENG can serve as a human-machine interface for a self-powered drone navigation system.

INTRODUCTION

Skin-attachable electronic devices with conformal and biocompatible adhesion to skin surfaces, often referred to as electronic skins (E-skins),^{1–3} are desired for compact and convenient human-machine interfaces (HMI) and can obtain accurate and reliable biological/physical information.^{4–8} To date, various critical E-skin components and systems have been developed. Among them, triboelectric nanogenerators (TENGs) have shown promise as an *in-situ* energy source for E-skins, as well as a means to detect and monitor human physical activities.^{9–12} TENGs can directly convert mechanical energy into electricity based on the coupling effect of contact electrification and electrostatic induction, with the advantage of structural simplicity, diverse material options, and high conversion efficiency.^{13,14} Hence, the utilization of E-skins with the autonomous powering ability and active sensing capacity is of great significance for the realization of a self-powered mechanosensation HMI system.

Another important and fairly unique element of the E-skins is its ability to be directly adhered to the skin, with strong yet reversible bonding. Conventional adhesive patches studied for E-skins mainly include bioinspired microstructured adhesives, pressure-sensitive adhesives, and chemical adhesives. The bioinspired microstructured adhesives, such as gecko foot-inspired micropillar arrays¹⁵ or suction cup

Progress and potential

Reversible stickers play an important role in skin-attachable electronics. Triggerable adhesives responsive to stimuli, such as pH, UV, and chemical agents, may not be benign to humans and have limited applications on E-skins. The present work provides a new debonding-on-demand biocompatible adhesive with a narrow transition temperature span and large modulus change, demonstrating skin temperature-triggered conformal adhesion and room temperature-triggered easy detaching. Base on the reversible adhesive, a debonding-on-demand triboelectric nanogenerator is demonstrated as a human-machine interface for a self-powered drone navigation system. The obtained adhesion is responsive to mild, efficient, and accessible stimuli, such as cold water, making it a promising candidate for many applications for smart artificial skins, soft robots, and self-powered biomechanical monitoring systems.

architectures inspired by octopus suckers,^{16,17} demonstrate strong adhesion on smooth surfaces, while their adhesion on uneven and soft surfaces is poor. Thus, they may not be a good option for skin which is uneven, soft, and often hairy. Pressure-sensitive adhesives,¹⁸ which bind to surfaces upon contact and light pressure, tend to have inadequate adhesion leading to premature detachment. Chemical adhesives, which form complementary functional groups, such as carbon-carbon,¹⁹ amide,²⁰ siloxane,²¹ and carbon-nitrogen²² with adherend, can offer strong and secure adhesion for E-skins, but could be difficult to remove after use. In addition, the removal process may trigger inflammatory responses that lead to irritation and pain.²³ Since the covalent bonds are broken and cannot be reformed once the patch is removed, E-skins based on chemical adhesion are single-use devices.

The ideal E-skins should be capable of repeated attachments and detachments, similar to a wristwatch, and, as a result, reversible debonding-on-demand (DoD) adhesives have gained attention for wearables and skin-attachable E-skins. Chen et al.²⁴ introduced a bio-adhesive hydrogel that can be detached by cleaving both physical amide bonds and covalent disulfide bonds using an aqueous solution containing sodium bicarbonate and glutathione. This DoD adhesive demonstrates both tough adhesion and triggerable detachment. However, the detachment requires the specially formulated solution for triggering and the hydrogel adhesive cannot be reused without drying out the absorbed water. Other detachable adhesion materials have also been reported with noncovalent or dynamic covalent adhesion bonds that are cleaved in response to external stimuli, such as UV light,^{25,26} chemicals,^{27,28} humidity,^{29,30} magnetic fields,³¹ and electrical current.³² While these triggers could provide switchable adhesion properties with adequate on/off adhesive strength ratios, they require external stimuli that may be inaccessible or harsh for use on human skin, and limited to particular types of substrate.

We have developed a new reversible DoD biocompatible skin adhesive that utilizes the temperature difference between the human body and its surrounding environment. This bistable adhesive polymer (BAP) is relatively stiff and not adherent at ambient temperature but soft and sticky at increased temperatures. The BAP is a copolymer comprising stearyl acrylate (SA) and tetradecyl acrylate (TA) in a chemically crosslinked elastomer network. The crystalline melting transition of the mixed stearyl and tetradecyl chains between 26°C and 32°C leads to a large modulus reduction and high flowability. BAP films are sticky above 32°C, allowing E-skins to adhere to skin and stay attached during routine activities. It becomes non-tacky and easily removable from the skin at temperatures below 26°C, which are easily obtainable using tap water.

To demonstrate the potential of BAPs for E-skin applications, a DoD-TENG was fabricated using the BAP as the DoD substrate. The TENG function was generated using a dielectric elastomer as the electrification layer and an ionic hydrogel as the electrode. The DoD-TENG device is optically transparent and mechanically compliant during the on-skin usage, and becomes opaque and relatively stiff when freestanding in the air. The capabilities of this DoD-TENG were demonstrated through a human-machine interface for self-powered sensor networks and mechanosensitive communication systems.

RESULTS AND DISCUSSION

Skin temperature-triggered, DoD mechanism of BAP films

The BAP polymer was synthesized by copolymerizing a mixture of SA, TA, and a long-chain urethane diacrylate (UDA) (CN9021) oligomer via photo-polymerization. The

¹Department of Materials Science and Engineering, Henry Samueli School of Engineering and Applied Science, University of California, Los Angeles, Los Angeles, CA 90095, USA

²Department of Molecular and Medical Pharmacology, University of California, Los Angeles, Los Angeles, CA 90095, USA

³College of Light Industry Science and Engineering, Tianjin University of Science and Technology, Tianjin 300457, China

⁴These authors contributed equally

⁵Lead contact

*Correspondence: qpei@seas.ucla.edu
<https://doi.org/10.1016/j.matt.2021.03.003>

molecular structures of these key ingredients are shown in [Figure S1](#). Acrylate with long alkyl side-chain SA was selected in the copolymer system as it exhibits a narrow melting temperature range (T_m) between 47°C and 50°C.³³ Due to the fact that a shorter alkyl chain could help decrease the melting temperature of *n*-alkyl acrylates, TA was added to lower the phase transition temperature to the range of human skin temperature. Acrylate was chosen over methacrylate for the polymerization segment due to the smaller steric hindrance for crystallization, which facilitates adequate modulus change in the phase transition period.³⁴ With SA and TA alone, the amorphous state of their polymers are gel like, which shows low mechanical strength, and they are inefficient in retaining the shape. To solve this problem, instead of utilizing a short-chain crosslinker, long-chain UDA was chosen to form the elastomeric network as the homopolymer of UDA has a modestly low modulus (0.827 MPa) and a large elongation at breakage of 1,100%.³³ The addition of UDA improved the toughness without increasing the modulus of the BAP for the adhesive state, which also reduces the possibility of cohesion failure with residue left on the adherend during the peeling process. Unlike the commonly used shape memory polymer adhesives, whose crystallizable segments are crosslinked in the network,^{35–37} the BAP film's crystallizable moieties are freely dangling along with the backbone polymer, as shown in [Figure S2](#). With this configuration, the mobility of the long alkyl chain would be less restricted, contributing to the ability of the BAP film to organize into an ordered crystalline structure. This phenomenon would lead to narrow transition temperature span, high crystallinity of the cold state, and efficient adhesive/non-adhesive modulus change, which are advantageous for DoD wearable applications.

The bonding/debonding mechanism of the BAP is shown in [Figure 1A](#). The adjustable adhesive behavior is ascribed to the skin temperature-triggered semicrystalline-to-amorphous transition ([Figure 1Ai](#)). In the SA/TA-UDA copolymer-based BAP, the crystalline aggregates of the SA and TA moiety act as hard segments in the copolymers and lead to a rigid phase when $T < T_m$. As the crystalline long alkyl side chains melt at increased temperatures, the rigid polymer becomes soft, with the amorphous stearyl and tetradecyl chains acting as the matrix plasticizer. Unlike the semicrystalline state, the amorphous state ensures high flowability, and the film can readily flow and conform to the target surface. Meanwhile, the polymer's low modulus and low viscosity, enabled by its soft alkyl chains, give the film a property of high energy dissipation.³⁸ During peeling and deformation, the stretching force is distributed over a large body of the film, thus mitigating the tendency of cleaving the adhesion front or rupturing the local structure.³⁹ Therefore, the BAP exhibits physical adhesive characteristics above T_m and shows a thread-like microstructure at the peeling interface ([Figure 1Aii](#)).

The transition temperature of the BAP was tuned by modifying the SA:TA weight ratio and measured via dynamic mechanical analysis (DMA). The test was conducted at a temperature ramping rate of 3°C/min across the phase transition temperature range and a mechanical loading frequency of 1 Hz. As illustrated in [Figure 1B](#), the semicrystalline-to-amorphous transition temperature decreases with an increase of TA due to its shorter alkyl chain compared with SA. At an SA:TA weight ratio of 2:3, the BAP has a narrow transition temperature range between 26°C and 32°C, which is just below the surface temperature of the skin, making it an ideal candidate for a skin temperature-triggered bistable polymer. The film possesses a steep stiffness change of $\sim 1,000$ times from a storage modulus (G') of about 30.8–0.03 MPa. Once the transition is completed, the storage modulus does not change significantly with further temperatures increase. Differential scanning calorimetry results ([Figure S3](#)) are also provided, showing a T_m of approximately 33.1°C for the BAP film between the two cured phase transition materials, poly(SA) (55.3°C) and poly(TA) (26.6°C), which are consistent with the DMA results.

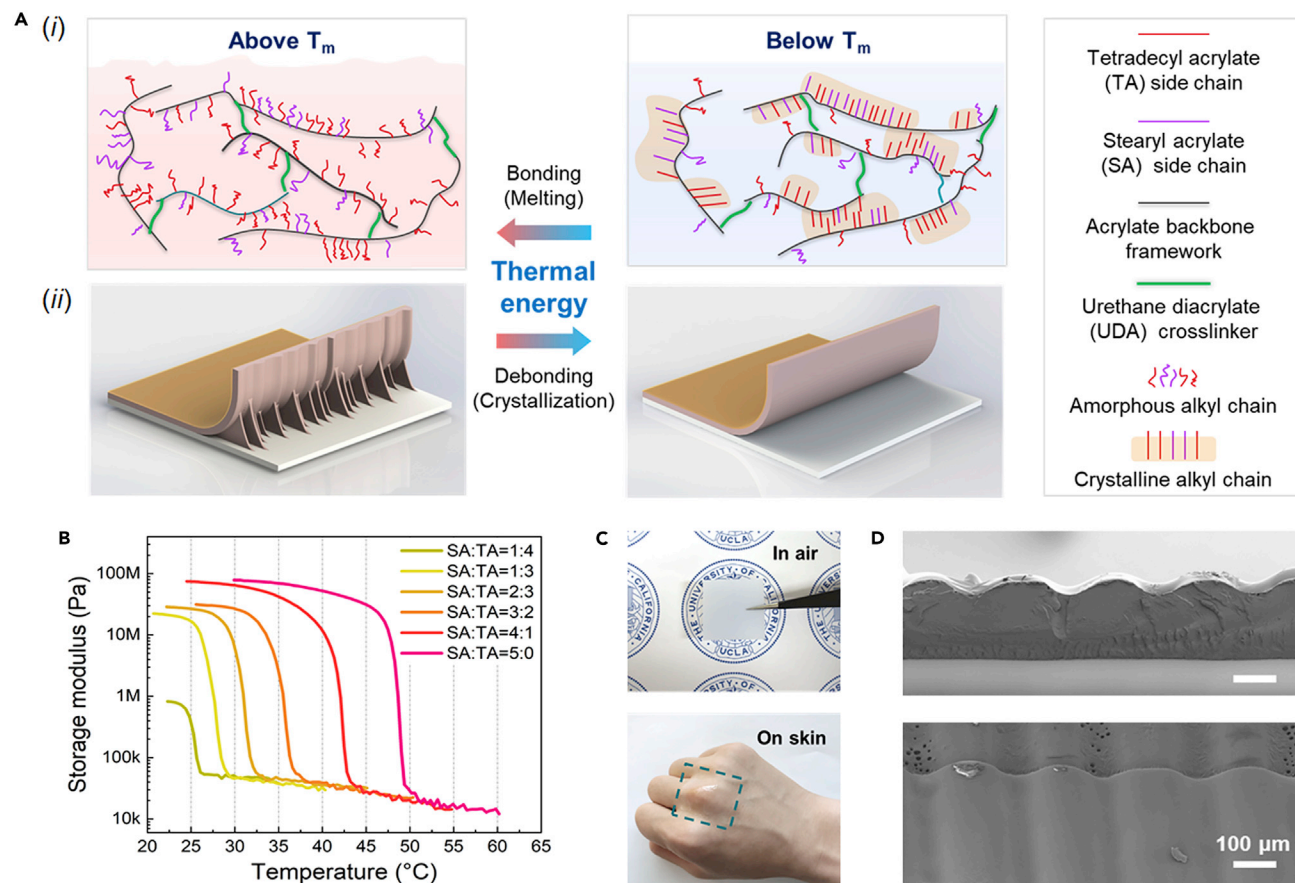


Figure 1. Skin temperature-triggered, debonding-on-demand mechanism of BAP films

(A) Schematic illustration of BAP's semicrystalline-to-amorphous phase transition of the linear alkyl chains (i) and the interfacial behavior during the peeling process (ii).

(B) Temperature-modulus curves of BAPs with different SA/TA ratios.

(C) Photographs of a BAP patch held in the air (upper) and attached to a hand (lower).

(D) SEM images taken at 90° and 45° angles of BAP films placed on the micro-grooved surface at heated temperature (40°C).

See also [Figures S1–S5](#).

The unique phase transition property of the BAP allows it to be handled as a free-standing film at room temperature, but conform to human skin along the highly curved contours of knuckles at skin temperature ([Figure 1C](#)). The patch could retain its position without delamination or tear despite the application of various external forces, such as tension, compression, and shear ([Figure S4](#)). The changes in the adhesion property and flowability of BAP under different temperatures are imaged by cross-sectional scanning electron microscopy (SEM) at 45° and 90° angles ([Figures 1D](#) and [S5](#)). BAP films are placed on a laser-cut PET micro-groove pattern substrate under ambient environment (21°C), and heated temperature (40°C), respectively. At room temperature, the BAP film maintains its original planar shape. At 40°C, it conforms smoothly and tightly along the microstructured grooves.

Bonding/debonding performance of the BAP films

To quantitatively assess the bonding strength of the BAP film, a standard 90° peeling test was conducted with a peeling rate of 50 mm/min. The schematic illustration of the test is presented in [Figure 2A](#). In a typical experiment, the bottom surface of the testing substrate is fixed onto the glass slide, while the BAP film

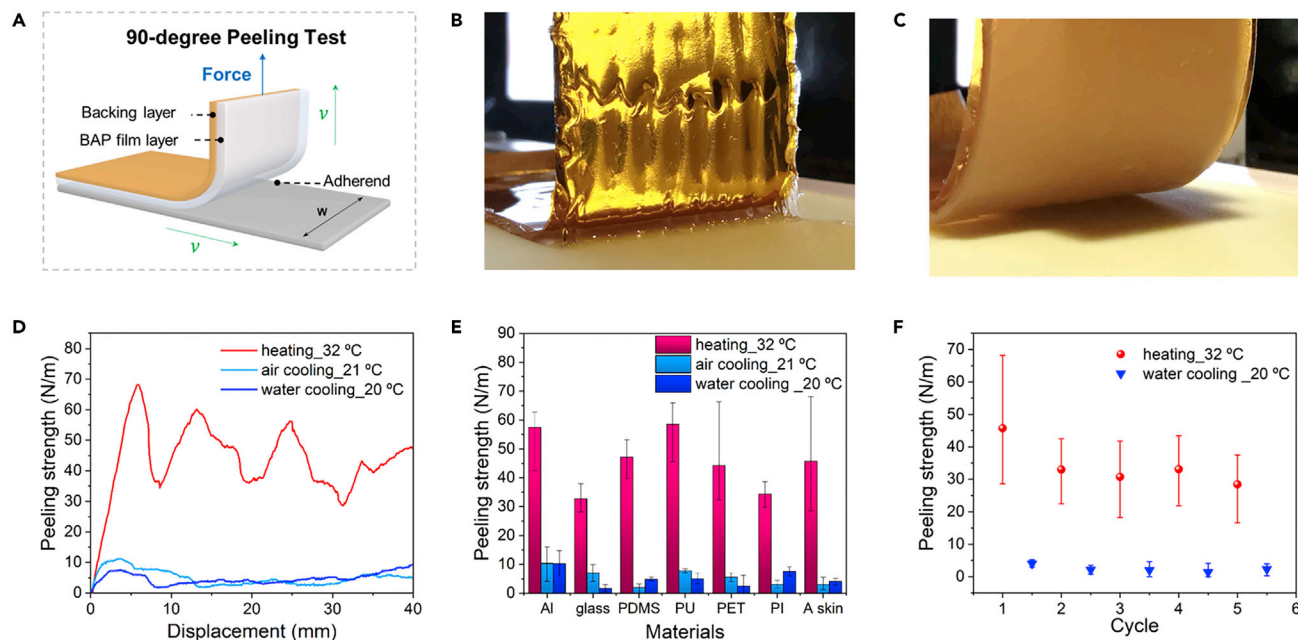


Figure 2. Bonding/debonding performance of the BAP films

(A) Scheme of 90° peeling test.

(B and C) Photographs of BAP films being peeled off from adherends at 32°C and 20°C after being cooled with tap water. A yellow Kapton film was used as the stiff backing for the BAP film.

(D) Representative force-displacement curves of BAP films detached from artificial skin under three circumstances, including heating to 32°C, cooling down to 21°C in air, and cooling down to 20°C in water, respectively.

(E) Measured peel strengths of BAP attached to diverse adherends.

(F) Measured peel strengths of the BAP-artificial skin system under periodical temperature change from 32°C to 20°C, illustrating the reusability of the BAP film.

See also [Figures S6–S9](#) and [Video S1](#).

of 1,000 μm thickness adheres to a thin stiff backing (polyimide, with a thickness of 90 μm), which prevents film elongation along the peeling direction. For BAP measured at 32°C, a typical adhesive thread-like microstructure is observed at the interface as the peeling propagates (Figure 2B). When the film is cooled down to 21°C, the interface between the BAP film and substrate is clear, which demonstrates poor adhesion performance, as depicted in Figure 2C, and the interface easily propagates along with the BAP film without kinking or deformation. When the BAP film is attached to the adherend, the polymer chains cause the intrinsic work of adhesion, the surface energy W_{ad} . Meanwhile, the BAP film around the interface is highly deformed and thus dissipates a significant amount of mechanical energy, which further contributes to the dissipation energy W_{dis} . Generally, W_{ad} is much lower than W_{dis} .¹⁹ The total peeling energy (W) of BAP-adherend bonding can be expressed as^{40,41}

$$W = W_{ad} + W_{dis} \quad (\text{Equation 1})$$

Since the dissipation energy is inversely proportional with the modulus of the DoD adhesive,⁴¹ when under transition temperature it is the surface energy W_{ad} that mainly contributes to the BAP film's peel strength, exhibiting a very low value. Whereas, when the film is heated above the transition temperature, low modulus and large deformation are developed in the bulk BAP film to give high values of dissipation energy W_{dis} .

The measured bonding strengths are shown in [Figure 2D](#). At 32°C, the peel strength between the BAP film and an artificial skin is 45.7 N/m, which drops to 3.0 and 4.1 N/m when cooled down to room temperature with ambient air and water, respectively. The value of the peeling strength is calculated by dividing the peeling force (F) with the width of the film (w). The peeling curves at the heated state fluctuate somewhat periodically as the BAP needs to absorb sufficient energy along the peeling direction before the detachment with adherend takes place discretely ([Figure S6](#)). The relationship of peel strength and the BAP film adhesive is also investigated. As shown in [Figure S7](#), the peel strength of the BAP film is proportional to the thickness in the investigated region at increased temperature, while it maintains a low value after cooling in water. For a variety of other substrates ([Figure 2E](#)), the average peel strengths are similarly high (32.7–57.5 N/m). However, BAP films at room temperature bond poorly to the test surfaces regardless of the cooling method. Therefore, apart from application in skin-mounted devices, the BAP could also be utilized in other specific scenarios on a diverse set of substrates where adjustable adhesive force is required.

To examine the bonding/debonding stability of the BAP film for repeated uses, the peel strengths were measured at 20°C and 32°C for 6 cycles. It should be noted that the room temperature condition chosen here is provided by water cooling, which is convenient to implement in the lab and also a practical approach for skin-mounted electronics. As illustrated in [Figure 2F](#), the peel strength drops slightly at 32°C after cycle 1 and then remains steady thereafter. At 20°C, peeling strength remains at low values. Due to the inherent hydrophobic nature of the BAP film, the DoD adhesive is resistant to water, with unnoticeable swelling when placed in water. When BAP film bonded with artificial skin adherend is immersed in 32°C water 10 min before the 90° peeling test is conducted, no significant difference is observed before and after this process, as shown in [Figure S8](#), indicating that water, or sweat, does not significantly impact the adhesive strength of the BAPs. This is also indicative that the 20°C water cooling detaching process is derived from the low temperature rather than the interaction of the BAP with water.

The easy bonding and debonding on human skin are demonstrated in [Video S1](#). The 340 μm BAP film is fairly stiff and easy to handle. As soon as the film makes contact with a human hand, it conforms to the epidermal structure. The film on the skin is difficult to peel off. When immersed in water for 1 min, it can be easily removed from the hand, without leaving residue or causing skin discomfort. The peeled off film exhibits a stiff nature. After shaking off the surface water or air drying, it can be mounted on the skin again and strong adhesion is observed. The DoD adhesion triggered by mild, efficient, and accessible stimuli (cold water), along with narrow temperature transition (6°C) and large modulus change (1000 times), make the BAP film an ideal material for wearable electronics. In the adhesive state, the peel strength of the 340 μm BAP film is adequate for conformal contact and adhesion with human skin under random motion, which guarantees the effectiveness of the human-machine interface and the accuracy of collected signals. In the non-adhesive state, the film could detach from human skin easily, which would not only reduce skin irritation and pain, but also keep the electronic device intact and stable without components dislocation.

Biocompatibility tests of the BAP film were conducted, considering its conformal and intimate contact with human skin during usage. [Figure S9](#) shows fluorescent staining images of the live/dead cell assay of NIH3T3 cells after being cultured with (a) and without (b) BAP film for 1 day. The experimental samples and control samples

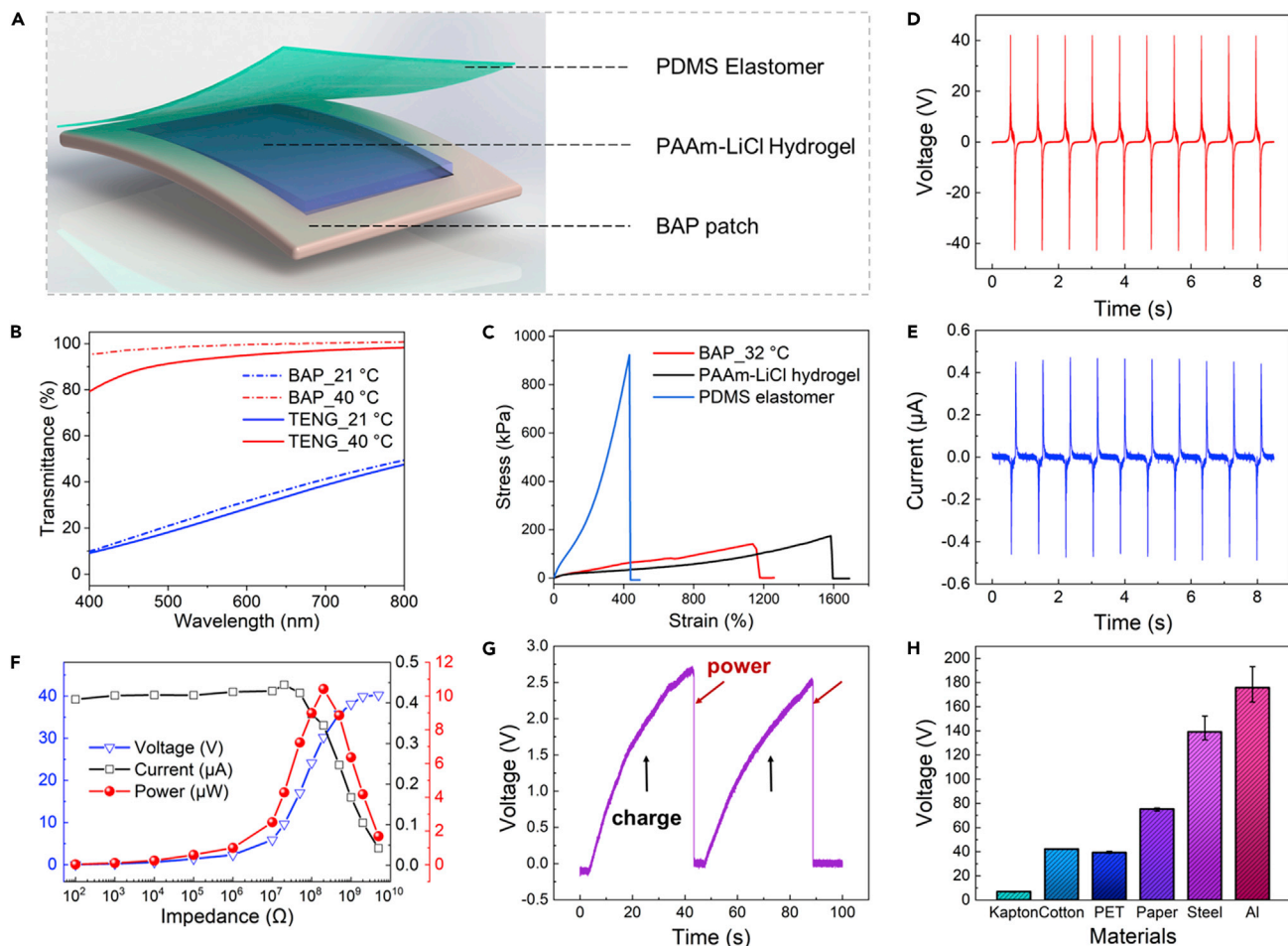


Figure 3. Optical, mechanical, and electrical performance of DoD-TENG

(A) Scheme of the DoD-TENG with sandwiched structure.
 (B) Transmittance of BAP and DoD-TENG tested at both room temperature (21°C) and after heating to 40°C.
 (C) Uniaxial tensile test of PDMS elastomer, PAAm-LiCl hydrogel, and BAP measured at 32°C.
 (D and E) Voltage and current output waveform of the DoD-TENG.
 (F) The relationship between power output and load resistance.
 (G) Voltage profile of a 0.5 μF capacitor being charged by DoD-TENG and used to power a thermistor.
 (H) The triboelectrification properties of various materials against DoD-TENG.

See also [Figures S10–S18](#).

show a negligible quantitative difference of live and dead cells, demonstrating a good cytocompatibility of the BAP film.

Optical, mechanical, and electrical performance of DoD-TENG

A single-electrode mode DoD-TENG with a sandwich-like architecture was designed to demonstrate the potential of the BAP in E-skin devices, as shown in [Figure 3A](#). The DoD-TENG consists of a silicone rubber layer (polydimethylsiloxane [PDMS]) acting as the tribo-negative material, a polyacrylamide (PAAm) hydrogel containing lithium chloride as the ionic current collector (PAAm-LiCl hydrogel), and the BAP as the DoD substrate. The fabrication process is described in the [experimental procedures](#) and [Figure S10](#), and the working principle, including contact triboelectrification and electrostatic induction is shown in [Figure S11](#). One major concern about the use of a hydrogel is dehydration over time, which would deteriorate the electrode's ionic

conductivity and mechanical elasticity. To increase its water retention capacity, a high initial dissolved salt concentration (0.6 mg/mL) and encapsulation structure are designed, with the DoD-TENG showing no significant weight changes in a 7-day period stored in the ambient environment (Figure S12).

The transmittance of DoD-TENGs was measured and the results are shown in Figure 3B. In the heated state (40°C), the BAP shows an average transmittance of 99.1% in the visible spectrum (400–800 nm), and the corresponding DoD-TENG shows transmittance of 93.4%. In contrast, the BAP and DoD-TENG tested at room temperature (21°C) showed an average transmittance of 30.9% and 28.4%, respectively, which are significantly lower than those at increased temperatures. The large change in transmittance is due to the reversible semicrystalline-to-amorphous transition of the SA and TA moiety, where the semicrystalline state ($T < T_m$) is opaque due to Rayleigh scattering, while the amorphous state ($T > T_m$) is transparent. The transmittance of PDMS elastomer (98.8%) and PAAm-LiCl hydrogel (94.9%) are also provided in Figure S13. The high transparency of the DoD-TENG device on the skin can be a useful feature. For instance, the user may choose to keep the low profile of the device, or color it for fashion or expression.

Uniaxial tensile tests of the elastomers used in the device were performed to evaluate the mechanical properties of the DoD-TENGs (Figure 3C). At 32°C, the BAP elastomer had ultimate tensile stress of 141.2 kPa at a strain of 1,138%, while the PDMS elastomer and the PAAm-LiCl hydrogel exhibit an elongation at break at around 433% and 1,584%, respectively. The high elongations of each component guarantee the stretchability of DoD-TENG utilized on skin. It can, therefore, be suggested that ultrahigh stretchability and transparency could be achieved simultaneously when the film is attached on the skin with the temperature above T_m . The stress-strain curves of BAP measured at room temperature (21°C) are also provided in Figure S14. At room temperature, the BAP reaches a fracture strain at 250%, which is just 22% of that of BAP at 32°C.

To test the output signal and electricity generation of the DoD-TENG, periodic contact, and separation movements between the device and its contact object were conducted. As demonstrated in Figures 3D and 3E, when utilizing cloth as the positive triboelectric material, the peak open-circuit voltage and the peak short-circuit current was 42 V and 0.46 μ A, respectively, with the input impedance of the oscilloscope being 100 M Ω . The voltage and current waveform depict a typical triboelectric output with a high signal-to-noise ratio, which shows its ability to be used as high-accuracy, self-powered sensors. By varying the external resistance, it was observed that the output voltage of the device increased with the increase of external loads with the output current showing a reverse trend according to Kirchhoff's law. The maximum areal power density output was measured to be 17.37 mW/m² at an approximately matched impedance of 200 M Ω , as shown in Figure 3F.

The charging curves for different capacitors are displayed in Figure S15. The tests were performed by using a finger to tap a contact area of 3 \times 2 cm² at a frequency of 1–2 Hz. Figure 3G shows the real-time charge/discharge curves of capacitors powering a thermistor. The voltage of the capacitor reached 2.6 V in 40 s and can later drive the thermistor, which is used to detect the surrounding temperature. By measuring the decay time constant of the discharge curve, the ambient temperature when testing was calculated as 20.98°C. Subsequently, the capacitor can be charged again and can power the thermistor repeatedly.

Due to the feasibility of contact electrification between any two different layers, the DoD-TENG can generate voltage/current outputs from the relative motion with many other materials. Various materials were tested and the corresponding open-circuit voltages are recorded in [Figure 3H](#). The voltage amplitude and polarization depend on the relative ability of a material to lose or gain electrons when in contact with its counterpart adopted in this work, i.e., PDMS. [Figure S16](#) shows the details of the triboelectric output of a variety of tribo-positive materials against the tribo-negative PDMS layer. The results show that the voltage output ranges from 6.9 to 175.8 V, with the largest value coming from an aluminum thin film. As a result, other materials can also serve as the triboelectric pair with the DoD-TENG, indicating potential applications in other scenarios, such as textile-based electronics.

The stability and reusability of DoD-TENG in water were tested by measuring the electrical performance before and after immersing the device in water for 5 min ([Figure S17](#)). The results show that the voltage output was not impaired after repeated contact with water, demonstrating the feasibility of using water to cool down the device to detach and reuse. The durability of the DoD-TENG was also tested over long-term motion cycles. After $\sim 4,300$ cycles (for 1 h) of repeated contact-separation motion, the open-circuit voltage showed a low output fluctuation ([Figure S18](#)).

DoD-TENG used for a self-powered mechanosensitive communication system

The combination of self-powered sensing ability, stretchability, conformability, and the reversible DoD property of the DoD-TENG allowed the fabrication of a wearable HMI. A wearable drone navigator (WDN) was fabricated via the integration of four DoD-TENGs to provide navigation instruction to a commercial drone (rotations and directions) ([Figure 4A](#)). The WDN was attached to the user's fingers ([Figure 4B](#)). Index, middle, ring, and little fingers were coded to signal 2^1 , 2^2 , 2^3 , 2^4 with a micro-controller for real-time communication, respectively. As depicted in [Figure 4C](#), with simple touching interactions on the WDN, the corresponding DoD-TENG generates an obvious output signal. The signal was detected through a multi-channel data acquisition method, and processed via a MATLAB script. After processing, real-time statistics were sent to the drone and instructed on its flight movement. The flight information was also displayed on a graphical user interface on the screen for feedback ([Figure 4D](#)). The motions of the drone were controlled by different commands, and the corresponding output voltage waveforms with the time sequence of each channel are shown in [Figure 4E](#), indicating the feasibility of our sensing system for drone flight manipulation. A value of "0011" was needed to input a "Take Off" order and required a simultaneous touch of the ring finger (2^3) and the little finger (2^4). For sending a "↑" (go forward) order, a value of (1000) was needed, which was given by a single touch of the index finger (2^1). Other orders were based on the same mechanism. The various flight movements were successfully carried out as shown in [Video S2](#) and [Figure S19](#). We conclude that the DoD-TENG-based drone navigator can achieve human-machine interaction with high accuracy and low delay, and the device meets the requirements for convenient wearing and accurate manipulation.

Conclusions

In conclusion, the BAP has successfully been explored as a DoD biocompatible skin adhesive, utilizing the temperature difference between the human body and the ambient environment. The stearyl and tetradecyl long alkyl chains attached to an elastomer network undergo a semicrystalline-to-amorphous transition between 26°C and 32°C , resulting in high flowability and large energy dissipation. Topological adhesion to a variety of substrates, including artificial skin and human skin, are

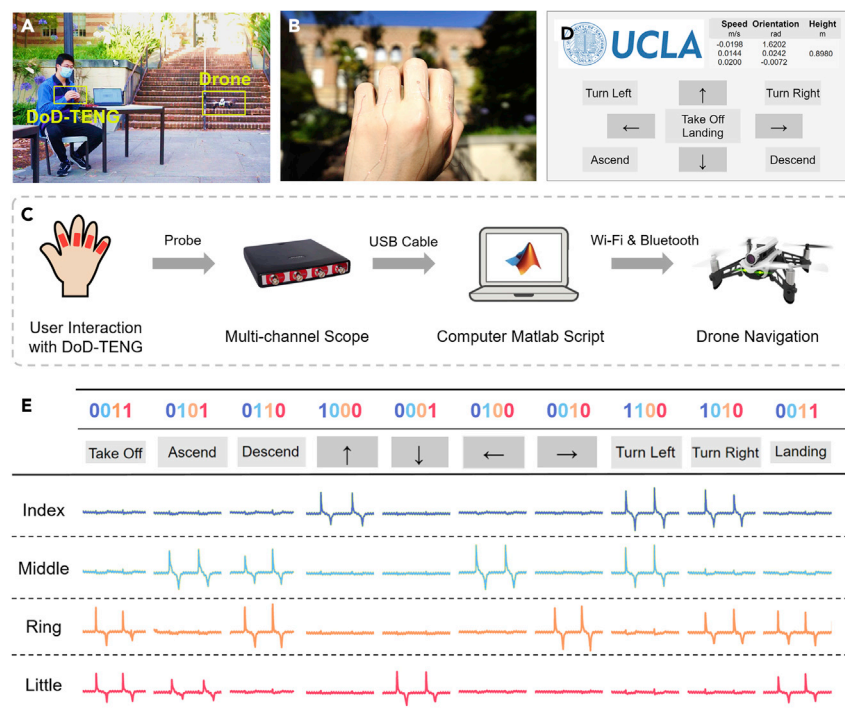


Figure 4. DoD-TENG used for a self-powered mechanosensitive communication system

(A) Photograph of the real-time drone navigation with DoD-TENG utilized as the command input. (B) Photograph of a wearable drone navigator made of four DoD-TENGs attached on human fingers.

(C) Scheme diagram of the DoD-TENG-based self-powered drone navigation system, including input, output, and processing units. The signal is detected through a multi-channel data acquisition method, and processed via a MATLAB script. After processing, real-time statistics are sent to the drone instructing its flight movement.

(D) Screenshot of the graphic user interface on the screen for information feedback.

(E) Voltage waveforms of different inputs and their corresponding flying orders. Index, middle, ring, and little fingers are coded to signal 2^1 , 2^2 , 2^3 , and 2^4 . The motions of the drone are controlled by a combination of different commands, and the corresponding output voltage waveforms are generated with the time sequence of each channel.

See also [Figure S19](#) and [Video S2](#).

strong at skin temperature, while detaching is made easy by cooling to the ambient environment with water and air. The BAP film becomes ultrasoft, conforms tightly to the skin, and adheres strongly. It can easily be detached after immersing in water for 1 min. A highly stretchable and transparent DoD-TENG was fabricated using a BAP as the DoD substrate, a PDMS elastomer as the electrification layer, and a PAAm-LiCl hydrogel as the electrode. Based on the single-electrode working mode, the E-skin device produces an open-circuit voltage of 42 V and a maximum matching peak power density of 17.37 mW/m². A human-machine interface was also demonstrated for self-powered drone navigation systems. This demonstrates the potential applications of the BAP for a wide range of smart artificial skins, soft robots, and self-powered biomechanical monitoring systems.

EXPERIMENTAL PROCEDURES

Resource availability

Lead contact

Further information and requests for resources and reagents should be directed to and will be fulfilled by the lead contact, Qibing Pei (qpei@seas.ucla.edu).

Materials availability

The materials generated in this study are available from the lead author upon reasonable request.

Data and code availability

The data used to support the findings of this study are available from the lead author upon reasonable request.

Fabrication of BAP

BAP was prepared by mixing SA/TA and UDA oligomers with a weight ratio of 80%:20%. The weight ratio of SA to TA was tuned to investigate the transition temperature. After adding 0.5% of DMPA as a photoinitiator, the entire HA/TA-UDA mixture was sonicated for 30 min before injecting into a glass mold. Then, UV light irradiation was adopted to initiate the polymerization.

Fabrication of the PAAm-LiCl hydrogel solution

The ionic hydrogel was synthesized by dissolving 4 g acrylamide (AAm) monomer and 6 g lithium chloride (LiCl) in 10 mL deionized water; 0.1 mg/mL of the crosslinker *N,N*-methylenebisacrylamide (MBAA), and 5 μ L/mL of the photoinitiator 2-hydroxy-2-methylpropiophenone (1173), with respect to the weight of the DI water, were mixed and sonicated for 10 min before use.

Fabrication of DoD-TENG

[Figure S10 \(supplemental information\)](#) schematically illustrates the detailed fabrication process of the DoD-TENG. The DoD-TENG consists of the PAAm-LiCl hydrogel solution sandwiched between the bonding/debonding BAP substrate and the negative electrification PDMS layer. The BAP precursor is injecting into a rectangular groove mold with 340 μ m Pi tape as a spacer before UV curing. Then the PAAm-LiCl hydrogel solution was injected into the cavity, and further cured by UV. For a better connection of the hydrogel electrode with external circuits, the wire for signal readout is immersed in the hydrogel solution, which would be cured and bonded inside the hydrogel. Then, the PDMS elastomer layer was fabricated by blade coating a well-mixed mixture of commercially available Silicone ELASTOSIL 7670A part A and part B (with a weight ratio of 1:1) on the prepared hydrogel layer. Finally, it was cured at 80°C for 2 h. All the devices used in the work are 3 \times 2 cm.

Setup of the human-machine interface using DoD-TENG for drone navigation

The triboelectric voltage signals generated from the DoD-TENG by tapping fingers were measured using a four-channel HS4 Scope connected to a computer. The measurement was controlled by a MATLAB script with an interval of 0.5 s, and the transmitted signal sections were also analyzed in a real-time manner parallel to the measurement. As a result, the input of finger gestures was converted to ten navigation commands of the drone under the binary coding rule narrated in the article. Then the navigation commands were sent to the drone through Wi-Fi and Bluetooth, with the flight parameters and attitude of the drone fed back and shown on the graphical interface.

Biocompatibility test of the BAP film

In a certified A2 biosafety cabinet, BAP films were placed in the standard 24-well cell culture plate after ethanol/UV sterilization. A total of 100,000 NIH3T3 mouse fibroblast cells were seeded in each well and cultured in Dulbecco's modified Eagle's medium with 10% fetal bovine serum supplemented with penicillin and streptomycin. The cell cultures were placed in a cell incubator at 37°C and 5% CO₂ for 1 day. Then, a live/dead cell assay was performed using Hoechst 33342 and ethidium homodimer-III

(EthD-III), in which the nuclei of all live or dead NIH3T3 mouse fibroblast cells were stained blue by Hoechst 33342 and dead cells were stained red by EthD-III.

Characterization and measurements

Mechanical properties were measured on a dynamic mechanical analyzer (TA Instruments RSAIII). Dynamic temperature sweep tests were conducted at a temperature ramping rate of 3°C/min and a frequency of 1 Hz from 21°C to 60°C. The stress-strain curves were obtained at room temperature and 32°C at a stretching rate of 0.25 mm/s. The transition temperature of the BAP film and the individual components were measured using a PerkinElmer differential scanning calorimeter (DSC 8000) at a ramping rate of 15°C/min. To analyze the flowability of the BAP film, SEM images were taken by a scanning electron microscope (ZEISS Supra 40VP SEM). The peel strength of the BAP film was measured through a 90° peel test with a peeling speed of 50 mm/min using a mechanical testing machine (UniVert, CellScale). The temperature of the BAP film was measured using an infrared camera (ICI 9320P). A live cell microscope (Nikon 90i) was used to observe the fluorescent images of cells cultured with BAP films. A UV-vis spectrometer (Shimadzu PharmaSpec UV-1700) was used to measure the transmittance spectra of the materials and the DoD-TENG with respect to a glass slide over the range of 400–800 nm. A step motor (LinMot HF01-37) was used to provide the input of mechanical motions. For all testing of energy generation of the DoD-TENG, the pressure (100 kPa), speed (2 m/s), and frequency (1.2 Hz) of the step motor was fixed. The voltage was recorded using a TiePie Handyscope HS4 four-channel high-resolution oscilloscope, and the current was recorded using a Keithley electrometer 6514. The force applied by the motor was detected using a Mark-10 force gauge.

SUPPLEMENTAL INFORMATION

Supplemental information can be found online at <https://doi.org/10.1016/j.matt.2021.03.003>.

ACKNOWLEDGMENTS

M.G. acknowledges the support by the Tianjin Nature Science Foundation (grant no. 18JCQNJC76800) and the “Research Plan Program” of Tianjin Municipal Education Commission (grant no. 2018KJ095). The authors acknowledge the use of instruments at the Electron Imaging Center for NanoMachines supported by NIH (1S10RR23057 to ZHZ) and CNSI at University of California, Los Angeles. The authors give thanks for help from Prof. Jun Chen and to Xun Zhao for the assistance with electrical signal measurement.

AUTHOR CONTRIBUTIONS

Conceptualization, M.G., H.W., and Q.P.; methodology, M.G. and H.W.; investigation, M.G., H.W., Z.X., Y.L., J.H., and S.W.; writing – original draft, M.G. and H.W.; writing – review & editing, Q.P., R.P., X.H., S.W., and J.H.; funding acquisition, Q.P.; resources, Q.P., X.H., and L.W.; supervision, Q.P.

DECLARATION OF INTERESTS

Q.P., M.G., H.W., and Z.X. have applied for a United States provisional patent application related to this study. Other authors declare no competing interests.

Received: December 20, 2020

Revised: February 2, 2021

Accepted: March 2, 2021

Published: March 30, 2021

REFERENCES

- Ding, W., Wang, A.C., Wu, C., Guo, H., and Wang, Z.L. (2019). Human-machine interfacing enabled by triboelectric nanogenerators and tribotronics. *Adv. Mater. Technol.* **4**, 1800487.
- Jeong, J.-W., Yeo, W.-H., Akhtar, A., Norton, J.J.S., Kwack, Y.-J., Li, S., Jung, S.-Y., Su, Y., Lee, W., Xia, J., et al. (2013). Materials and optimized designs for human-machine interfaces via epidermal electronics. *Adv. Mater.* **25**, 6839.
- Lebedev, M.A., and Nicolesis, M.A.L. (2006). Brain-machine interfaces: past, present and future. *Trends Neurosci.* **29**, 536.
- Chortos, A., Liu, J., and Bao, Z. (2016). Pursuing prosthetic electronic skin. *Nat. Mater.* **15**, 937.
- Yang, J.C., Mun, J., Kwon, S.Y., Park, S., Bao, Z.N., and Park, S. (2019). Electronic skin: recent progress and future prospects for skin-attachable devices for health monitoring, robotics, and prosthetics. *Adv. Mater.* **31**, 1904765.
- Kim, D.-H., Lu, N., Ma, R., Kim, Y.-S., Kim, R.-H., Wang, S., Wu, J., Won, S.M., Tao, H., Islam, A., et al. (2011). Epidermal electronics. *Science* **333**, 838.
- Hwang, I., Kim, H.N., Seong, M., Lee, S.-H., Kang, M., Yi, H., Bae, W.G., Kwak, M.K., and Jeong, H.E. (2018). Multifunctional smart skin adhesive patches for advanced health care. *Adv. Healthc. Mater.* **7**, 1800275.
- Xu, C., Yang, Y., and Gao, W. (2020). Skin-interfaced sensors in digital medicine: from materials to applications. *Matter* **2**, 1414.
- Peng, X., Dong, K., Ye, C., Jiang, Y., Zhai, S., Cheng, R., Liu, D., Gao, X., Wang, J., and Wang, Z.L. (2020). A breathable, biodegradable, antibacterial, and self-powered electronic skin based on all-nanofiber triboelectric nanogenerators. *Sci. Adv.* **6**, 9624.
- Meng, K., Zhao, S., Zhou, Y., Wu, Y., Zhang, S., He, Q., Wang, X., Zhou, Z., Fan, W., Tan, X., et al. (2020). A wireless textile-based sensor system for self-powered personalized health care. *Matter* **2**, 896.
- Qian, C., Li, L., Gao, M., Yang, H., Cai, Z., Chen, B., Xiang, Z., Zhang, Z., and Song, Y. (2019). All-printed 3D hierarchically structured cellulose aerogel based triboelectric nanogenerator for multi-functional sensors. *Nano Energy* **63**, 103885.
- Wu, H., Su, Z., Shi, M., Miao, L., Song, Y., Chen, H., Han, M., and Zhang, H. (2018). Self-powered noncontact electronic skin for motion sensing. *Adv. Funct. Mater.* **28**, 1704641.
- Wang, Z.L. (2017). On Maxwell's displacement current for energy and sensors: the origin of nanogenerators. *Mater. Today* **20**, 74.
- Wu, C., Wang, A.C., Ding, W., Guo, H., and Wang, Z.L. (2019). Triboelectric nanogenerator: a foundation of the energy for the new era. *Adv. Energy Mater.* **9**, 1802906.
- Drotlef, D.-M., Amjadi, M., Yunusa, M., and Sitti, M. (2017). Bioinspired composite microfibers for skin adhesion and signal amplification of wearable sensors. *Adv. Mater.* **29**, 1701353.
- Chun, S., Kim, D.W., Baik, S., Lee, H.J., Lee, J.H., Bhang, S.H., and Pang, C. (2018). Conductive and stretchable adhesive electronics with miniaturized octopus-like suckers against dry/wet skin for biosignal monitoring. *Adv. Funct. Mater.* **28**, 1805224.
- Su, S., Wang, S., Li, L., Xie, Z., Hao, F., Xu, J., Wang, S., Guan, J., and Wen, L. (2020). Vertical fibrous morphology and structure-function relationship in natural and biomimetic suction-based adhesion discs. *Matter* **2**, 1207.
- Novikov, M.B., Borodulina, T.A., Kotomin, S.V., Kulichikhin, V.G., and Feldstein, M.M. (2005). Relaxation properties of pressure-sensitive adhesives upon withdrawal of bonding pressure. *J. Adhes.* **81**, 77.
- Yuk, H., Zhang, T., Lin, S., Parada, G.A., and Zhao, X. (2016). Tough bonding of hydrogels to diverse non-porous surfaces. *Nat. Mater.* **15**, 190.
- Li, J., Celiz, A.D., Yang, J., Yang, Q., Wamala, I., Whyte, W., Seo, B.R., Vasilyev, N.V., Vlassak, J.J., Suo, Z., and Mooney, D.J. (2017). Tough adhesives for diverse wet surfaces. *Science* **357**, 378.
- Liu, Q., Nian, G., Yang, C., Qu, S., and Suo, Z. (2018). Bonding dissimilar polymer networks in various manufacturing processes. *Nat. Commun.* **9**, 846.
- Saiz-Poseu, J., Mancebo-Aracil, J., Nador, F., Busqué, F., and Ruiz-Molina, D. (2019). The chemistry behind catechol-based adhesion. *Adv. Mater.* **58**, 696.
- Chen, X. (2017). Making electrodes stretchable. *Adv. Mater.* **1**, 1600029.
- Chen, X., Yuk, H., Wu, J., Nabzdyk, C.S., and Zhao, X. (2020). Instant tough bioadhesive with triggerable benign detachment. *Proc. Natl. Acad. Sci. U. S. A.* **117**, 15497.
- Gao, Y., Wu, K., and Suo, Z. (2019). Photodetachable adhesion. *Adv. Mater.* **31**, 1806948.
- Hohl, D.K., and Weder, C. (2019). (De)bonding on demand with optically switchable adhesives. *Adv. Opt. Mater.* **7**, 1900230.
- Kim, N., Kang, H., Lee, J.-H., Kee, S., Lee, S.H., and Lee, K. (2015). Highly conductive all-plastic electrodes fabricated using a novel chemically controlled transfer-printing method. *Adv. Mater.* **27**, 2317.
- Yang, J., Bai, R., and Suo, Z. (2018). Topological adhesion of wet materials. *Adv. Mater.* **30**, 1800671.
- Xue, L., Kovalev, A., Dening, K., Eichler-Volf, A., Eickmeier, H., Haase, M., Enke, D., Steinhart, M., and Gorb, S.N. (2013). Reversible adhesion switching of porous fibrillar adhesive pads by humidity. *Nano Lett.* **13**, 5541.
- Zhao, D., Zhu, Y., Cheng, W., Xu, G., Wang, Q., Liu, S., Li, J., Chen, C., Yu, H., and Hu, L. (2020). A dynamic gel with reversible and tunable topological networks and performances. *Matter* **2**, 390.
- Drotlef, D.-M., Blümler, P., and del Campo, A. (2014). Magnetically actuated patterns for bioinspired reversible adhesion (dry and wet). *Adv. Mater.* **26**, 775.
- Eisenhaure, J., and Kim, S. (2014). An internally heated shape memory polymer dry adhesive. *Polymers* **6**, 2274.
- Ren, Z., Hu, W., Liu, C., Li, S., Niu, X., and Pei, Q. (2016). Phase-changing bistable electroactive polymer exhibiting sharp rigid-to-rubbery transition. *Macromolecules* **49**, 134.
- Livshin, S., and Silverstein, M.S. (2007). Crystallinity in cross-linked porous polymers from high internal phase emulsions. *Macromolecules* **40**, 6349.
- Park, J.K., Nan, K., Luan, H., Zheng, N., Zhao, S., Zhang, H., Cheng, X., Wang, H., Li, K., Xie, T., et al. (2019). Remotely triggered assembly of 3D mesostructures through shape-memory effects. *Adv. Mater.* **31**, 1905715.
- Huang, Y., Zheng, N., Cheng, Z., Chen, Y., Lu, B., Xie, T., and Feng, X. (2016). Direct laser writing-based programmable transfer printing via bioinspired shape memory reversible adhesive. *ACS Appl. Mater. Inter.* **8**, 35628.
- Chen, C.-M., Chiang, C.-L., Lai, C.-L., Xie, T., and Yang, S. (2013). Buckling-based strong dry adhesives via interlocking. *Adv. Funct. Mater.* **23**, 3813.
- Creton, C. (2003). Pressure-sensitive adhesives: an introductory course. *MRS Bull.* **28**, 434.
- Baljon, A.R.C., and Robbins, M.O. (1996). Energy dissipation during rupture of adhesive bonds. *Science* **271**, 482.
- Gent, A.N., and Hamed, G.R. (1977). Peel mechanics of adhesive joints. *Polym. Eng. Sci.* **17**, 462.
- Kim, J., Kim, D.W., Baik, S., Hwang, G.W., Kim, T.-i., and Pang, C. (2019). Snail-inspired dry adhesive with embedded microstructures for enhancement of energy dissipation. *Adv. Mater. Technol.* **4**, 1900316.